Water-Soluble Calix [4] arenes as Inhibitors for the Corrosion of Aluminium in 2 M H₂SO₄ Solution

Hani El Moll[1,], Khalaf M. Alenezi[1], Mahmoud K. Abdel-Latif [2], Hatem Halouani[1], Mohamad M. EL-Deeb[2]*

[1] Department of Chemistry, Faculty of Science, University of Hail, 81451 Hail, P.O. Box 2440 Hail, KSA.
[2] Chemistry Department, Faculty of Science, Beni-Suef University, 62514 Beni-Suef, Egypt.
[*]E-mail: hanielmoll@gmail.com

Corrosion inhibition of aluminum in 2M H_2SO_4 solution in the presence of 5,11,17,23-tetrasulfocalix [4] arene (Calix-OH) and 5,11,17,23-tetrasulfo-25,27-bis (2-amino-ethoxy) calix [4] arene (Calix-NH₂) is examined using potentiodynamic polarization and electrochemical impedance spectroscopy measurements. Density function theory (DFT) calculations are used to investigate the relationship between the molecular structures of the studied compounds and their inhibition efficiencies. Results show that the presence of these two compounds in 2M H_2SO_4 solution inhibits the corrosion of aluminum without modifying the mechanism of the corrosion process as evidenced from shifting both the corrosion and the open circuit potentials of aluminum to more noble values as well as decreases its corrosion current density compared to its value in the blank solution. The maximum inhibition efficiency is found to be for Calix-NH₂. Moreover, the structure of aluminum/electrolyte interface in case of Calix-NH₂ behaves as more ideal capacitive rather than that in case of Calix-OH. The best fit adsorption isotherm is found to be Langmuir adsorption isotherm with physical nature. DFT calculations show that the presence of R-NH₂ group in Calix-NH₂ increases the electron density, so increases the electrostatic attraction with aluminum surface and consequently the protection efficiency

Keywords: Aluminum, Inhibition, Calixarene, DFT, EIS

1. INTRODUCTION

In the field of supramolecular chemistry, cavitands, such as calixarenes are of great interest because of their easy functionnalization/derivatization. [1, 2]. In fact, the presence of four to eight rings of phenol connected through methylene bridging moieties constitutes a circular platform capable of accepting up to eight functional groups on both upper (para position) and lower (OH groups) rims (fig. 1). Thereby, wide variety of functional calixarenes was obtained. [3, 4] Among them, water-

soluble macromolecules with important applications in corrosion inhibition for various metals and alloys. [5-7] In recent years, considerable attention has been devoted to anti-corrosion materials based on supramolecular macrocycles. These studies concentrate on the corrosion inhibition of mild steel in the presence of hydrochloric acid. [8, 9].
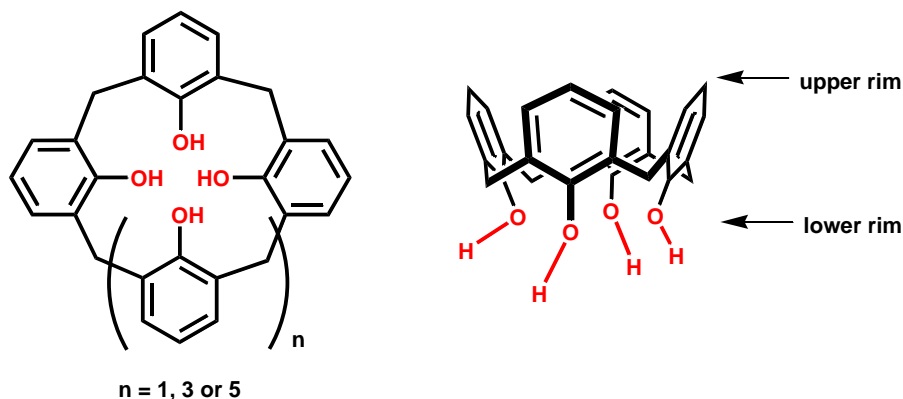

Figure 1. Drawing of calixarene (left). Illustration of the upper and lower rims of the generic calix[4]arene (right).

Aluminium and its alloys are very attractive for industrial uses, notably in aeronautics, transportation, construction, packing and electrical transmission. The importance of aluminium is due, mainly, to its low density and ability to resist corrosion by auto-passivation through the formation of a nano-metric film of aluminium oxide (Al_2O_3). [10, 11] However, the oxidation of aluminium should be controlled in the industrial processes, especially during the pickling of metal in acidic solutions such as sulfuric acid. The use of chemicals as corrosion inhibitors is one of the important research topics. In this context, El-Deeb and co-workers [11] studied the corrosion inhibition efficiency of aniline, *ortho*-toluidine and *ortho*-anthranilic acid in 2M sulfuric acid. They found better inhibition results in the presence of the *ortho*-substituted aniline by the donor group CH_3.

Calix[4]arene macrocycles (n = 4, fig. 1) are easily accessible by facile base-catalysed condensation reaction of phenol with the corresponding formaldehyde.[12, 13] Generally, they possess a hydrophobic cavity and a switchable hydrophobic-hydrophilic end with host-guest properties and tuneable structure for desirable properties.[14] Nowadays, their uses as corrosion inhibitors for metal and alloys are still limited. M. Kaddouri and co-workers [9] studied the corrosion inhibition of mild steel in 1M HCl at 308 K using four calix[4]arenes, mon-, di-, tri- or tetra-substituted by 4-imidazolylethylamidocarbonyl. They reached an inhibition efficiency of 94 to 100% at a concentration of 10^{-4} M.

The goal of our work is to investigate the inhibitory effect of 5,11,17,23-tetrasulfocalix[4]arene (Calx-OH) and 5,11,17,23-tetrasulfo-25,27-bis (2-amino ethoxy) calix[4]arene (Calx-NH$_2$) (fig. 2) for aluminum surface in 2M H_2SO_4 solution using electrochemical measurements. DFT calculations are used to clarify the obtained results.
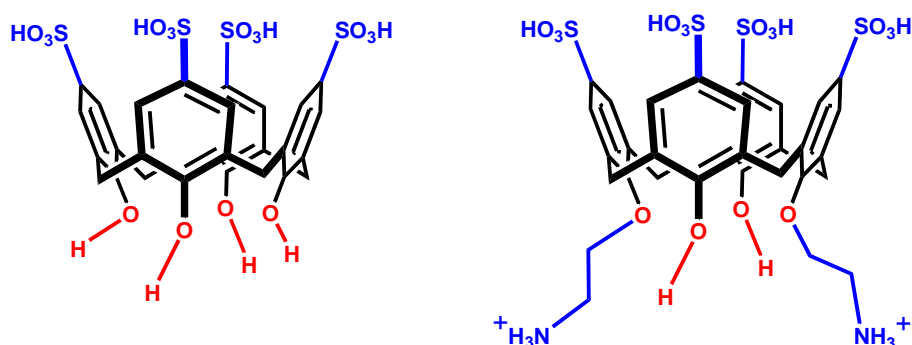
Figure 2. Drawings of 5,11,17,23-tetrasulfocalix[4]arene (left) and 5,11,17,23-tetrasulfo-25,27-bis(2-aminoethoxy) calix[4]arene (right)

2. EXPERIMENTAL SECTION

2.1. Materials

All starting materials such as 4-tert-butylphenol, formaldehyde solution, sodium hydroxide, aluminum chloride, phenol, bromoacetonitrile, potassium carbonate and borane tetrahydrofuran complex solution as well as the dry solvents are purchased from Afaq Sada Trading Est and used as received, concentrated sulfuric acid are provided from Merck Chemical Co., Germany. All solutions are prepared using deionized water (18.2 µS). Working electrode is made from aluminum rod (area = 1.0 cm^2) with 99.57% purity. Prior to use, it will be polished using emery papers with different grades, then washed and dried.

2.2. Synthesis

The 5,11,17,23-tetrasulfocalix[4]arene (Calix-OH) was prepared by debutylation of *p*-t-butylcalix[4]arene in presence of phenol and aluminium chloride followed by sulfonation in presence of concentrated sulfuric acid according to a previously reported method. [15, 16]

The 5,11,17,23-tetrasulfo-25,27-bis(2-aminoethoxy) calix[4]arene (Calix-NH$_2$) was prepared by debutylation of *p*-t-butylcalix [4] arene followed by the grafting of acetonitrile group on the lower rim of Calix[4]arene in the distal positions in presence of bromoacetonitrile and potassium carbonate. The cyano groups are than reduced in the presence of borane tetrahydrofuran complex solution. [15, 17] The resulting compound is sulfonated in the presence of concentrated sulfuric acid according to a previously described method. [18]

2.3. Electrochemical measurements

Electrochemical measurements are performed using standard three-compartment cell with the aluminum working electrode, Pt counter electrode, and Ag/AgCl reference electrode to which all potentials are referred. Potentiodynamic current–potential curves are achieved by changing the electrode potential automatically ±100 mV against the E$_{OCP}$ using scan rate of 1.0 mV s^{-1}. EIS measurements are carried out using AC signals of amplitude 5mV peak to peak at the E$_{OCP}$ in the

frequency range of 10 kHz to10 MHz. Potentiostat /galvanostat (Autolab PGSTAT 128N) and NOVA 1.10 software are used for recording and fitting the electrochemical experiment results.

2.4. Computational details

The ground state geometries of the studied compounds (Calix-OH and Calix-NH$_2$) are obtained using Gaussian 03 program package [19]. Density functional theory (DFT) using B3LYP/6-311G (d,p) level of the theory has been used for all the theoretical calculations: full optimization, frequency calculations and natural charge density [20-23]. The minima of the studied compounds have been confirmed using the frequency calculations in addition to calculate the total ground state energy with the zero-point energy (ZPE) correction at the same level of theory. The frequency calculations are used to ensure the minima structures. The molecular electrostatic (MEP) potential and electron density in three dimensional (3D) plots are investigated using the same level of theory.
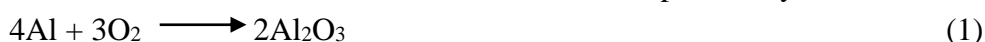
3. RESULTS AND DISCUSSION

3.1. Open circuit potentials

E_{OCP} values of aluminum electrode in 2 M H$_2$SO$_4$ solution in the absence and the presence of different concentrations (1 – 10 ppm) of both Calix-OH and Calix-NH$_2$ are determined after reaching the steady state versus time and tabulated in Table (1). Results show that, the values of E_{OCP} in the presence of the studied compounds are shifted towards more positive potentials compared to its value in the blank solution. The positive shifts in the E_{OCP} is attributed to the adsorption of these compounds on aluminum surface, which inhibits its anodic dissolution.

3.2. Potentiodynamic polarization measurements

Potentiodynamic polarization measurements of aluminum in 2M H$_2$SO$_4$ solution in the absence and presence of different concentrations (1 – 10 ppm) of Calix-OH and Calix-NH$_2$ compounds are studied ±100 mV against E_{OCP} at 30 °C with the scan rate of 1 mV/s as shown in Figure (3), while the electrochemical parameters and the calculated protection efficiencies [24, 25] are listed in Table (1). Results show that, the presence of both Calix-OH and Calix-NH$_2$ compounds shifts the corrosion potential (E_{corr}) of aluminum to more positive values as well as, decreases its corrosion current density (I_{corr}) compared to its values in blank solution. These results are attributed to their protective and inhibitive effect on the anodic dissolution of aluminum as previously discussed as follows [26, 27]:

$$4Al + 3O_2 \longrightarrow 2Al_2O_3 \qquad\qquad (1)$$

$$Al_2O_3 + nH_2O \longrightarrow Al_2O_3.(H_2O)_n \qquad\qquad (2)$$

$$Al_2O_3(2H_2O) + 3HSO_4^- + 3H^+ \longrightarrow Al_2[(SO_4)_3(H_2O)_n]_{ads} + 3H_2O \qquad (3)$$

The above results indicate that increasing the concentrations of Calix-OH and Calix-NH$_2$ compounds increase the aluminum surface coverage and consequently their inhibition efficiencies as illustrated in Table (1). This suggests that the adsorption of calixarenes on the aluminum surface blocks

the active sites, which usually cause the aluminum dissolution and the hydrogen evolution reactions [28].

Table 1. Electrochemical kinetic parameters of aluminum in 2M H_2SO_4 solutions at 30 ^oC in the absence or presence of different concentration of Calix-OH and Calix-NH_2 based on polarization measurements

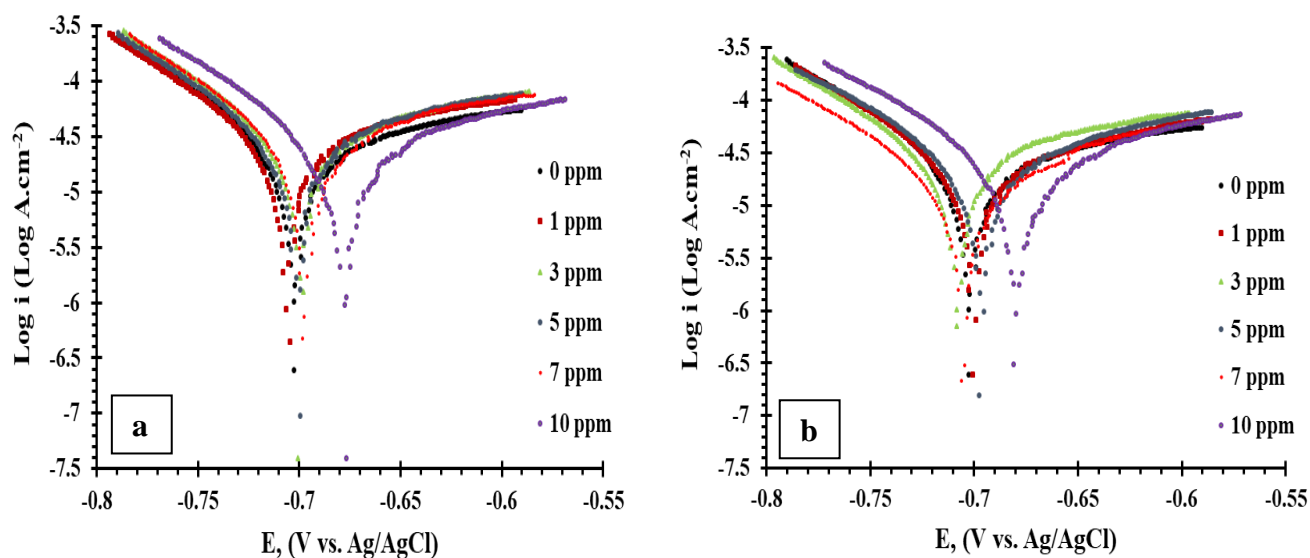| C, (ppm)	E_{ocp} (mV vs. Ag/AgCl)		E_{corr} (mV vs. Ag/AgCl)		I_{corr} ($\mu A\ cm^{-2}$)		θ		P%	
	Calix-OH	Calix-NH_2	Calix-OH	Calix-NH_2	Calix-OH	Calix-NH_2	Calix-OH	Calix-NH_2	Calix-OH	Calix-NH_2
0	-699		-709		169.2		----		----	
1	-699	-696	-705	-700	77.7	78.9	0.541	0.534	54.1	53.4
3	-698	-694	-700	-699	72.5	65.8	0.571	0.611	57.1	61.1
5	-691	-689	-698	-690	43.1	39.3	0.745	0.768	74.5	76.8
7	-685	-683	-697	-689	34.7	24.5	0.795	0.855	79.5	85.5
10	-671	-669	-680	-677	23.8	20.9	0.859	0.876	85.9	87.6

Figure 3. Potentiodynamic polarization curves of aluminum in 2M H_2SO_4 solution in (a) *x* ppm Calix-OH and (b) *x* ppm Calix-NH_2 at 30 °C with scan rate of 1.0 mV s^{-1}.

3.3. Impedance measurements

Adsorption of Calix-OH and Calix-NH_2 on aluminum/H_2SO_4 interface is investigated using EIS measurements. Figure (4) represents Nyquist plots of aluminum in 2 M H_2SO_4 solution in the absence and presence of 10 ppm Calix-OH or Calix-NH_2 at E_{OCP}. It can be seen that the presence of one semicircular capacitive loop for charge transfer mechanism [29] with different diameters in the

absence and presence of Calix-OH or Calix-NH$_2$. The diameter of this capacitive loop increases without any change in the shapes of the Nyquist plot in the presence of Calix-OH or Calix-NH$_2$, suggesting that the corrosion mechanism in the absence and presence of these compounds is not changed, as well as supports that the protection efficiency of these compounds towards the aluminum corrosion in H$_2$SO$_4$ solution takes place through their adsorption on the aluminum/ H$_2$SO$_4$ surface
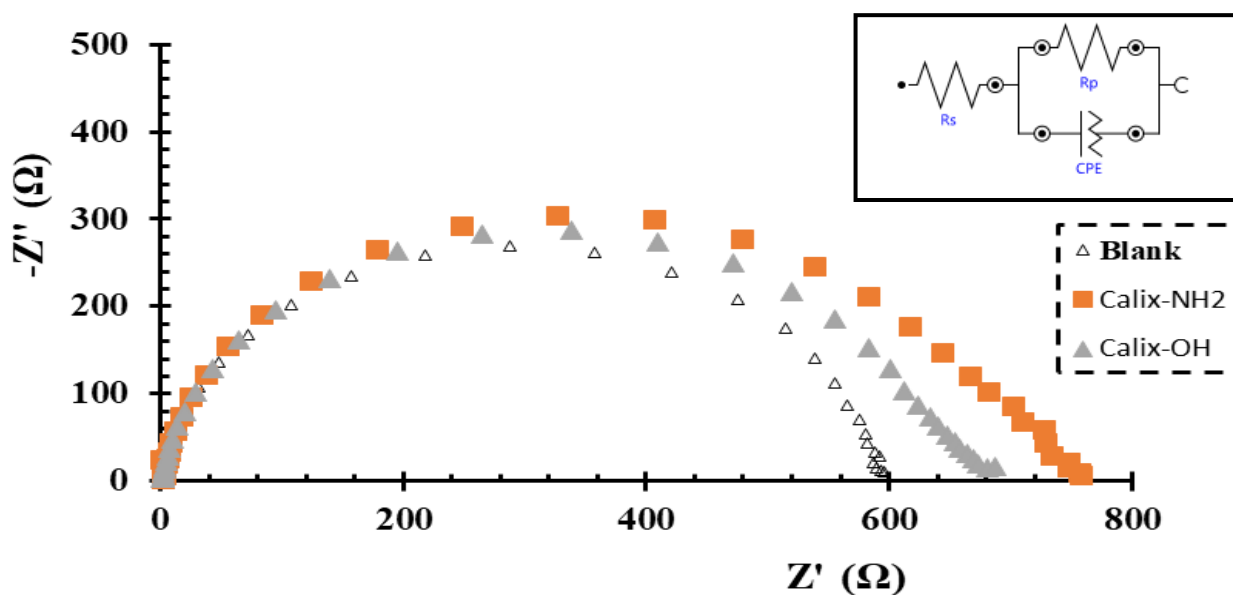

Figure 4. Nyquist plots of aluminum in 2M H$_2$SO$_4$ solution in the absence and presence of 10 ppm Calix-OH and Calix-NH$_2$ at E_{OCP}. The inset represents the electrical equivalent circuit model.

It can be seen from the inset of Figure (4) that, the Nequest plot of aluminum in 2M H$_2$SO$_4$ solution shows [$R(RQ)$] equivalent circuit with one-time constant is fitted to the experimental data obtained in the absence and presence of 10 ppm Calix-OH or Calix-NH$_2$ due to the dissolution of Al$_2$O$_3$ passive layer under the influence of its attack with the corrosive sulphate anions. Moreover, the replacement of the double layer capacitance (C_{dl}) with constant phase element (CPE) and phase shift (N) explains the surface heterogeneity, porosity and the adsorption of the studied compounds on the aluminum/H$_2$SO$_4$ interface [30]. The highest values of N accompanied with smallest values of CPE for aluminum/2M H$_2$SO$_4$ in the presence of 10 ppm Calix-OH ($N = 0.899$, $CPE = 10.2$ µMho) and Calix-NH$_2$ ($N = 0.904$, $CPE = 7.46$ µMho) compared to their values in the blank solution ($N = 0.895$, $CPE = 13.7$ µMho) is calculated from the fitted experimental measurements using Boukamp model [31].This means that, the aluminum/H$_2$SO$_4$ interface in case of Calix-OH and Calix-NH$_2$ behaves as more ideal capacitive rather than that in the absence of these compounds, which illustrates the role of Calix-OH and Calix-NH$_2$ in decreasing the roughness and increasing the homogeneity of the aluminum surface. Also, the higher value of (N) in case of Calix-NH$_2$ compared to its value in case of Calix-OH supports and agreements with the higher inhibition efficiency of Calix-NH$_2$ calculated from the polarization measurements.

3.4. Adsorption isotherms

Mechanism of the inhibition efficiencies of Calix-OH and Calix-NH$_2$ is illustrated from the hypothesis of their adsorption on aluminum/electrolyte interface. Therefore, the nature of the interaction between these compounds with aluminum/electrolyte interface is studied using different adsorption isotherms. Values of the surface coverage (θ) calculated from the potentiodynamic polarization measurements are fitted to different isotherms at 30 °C. The best fit is found to be with Langmuir adsorption isotherm as shown in Figure (5).
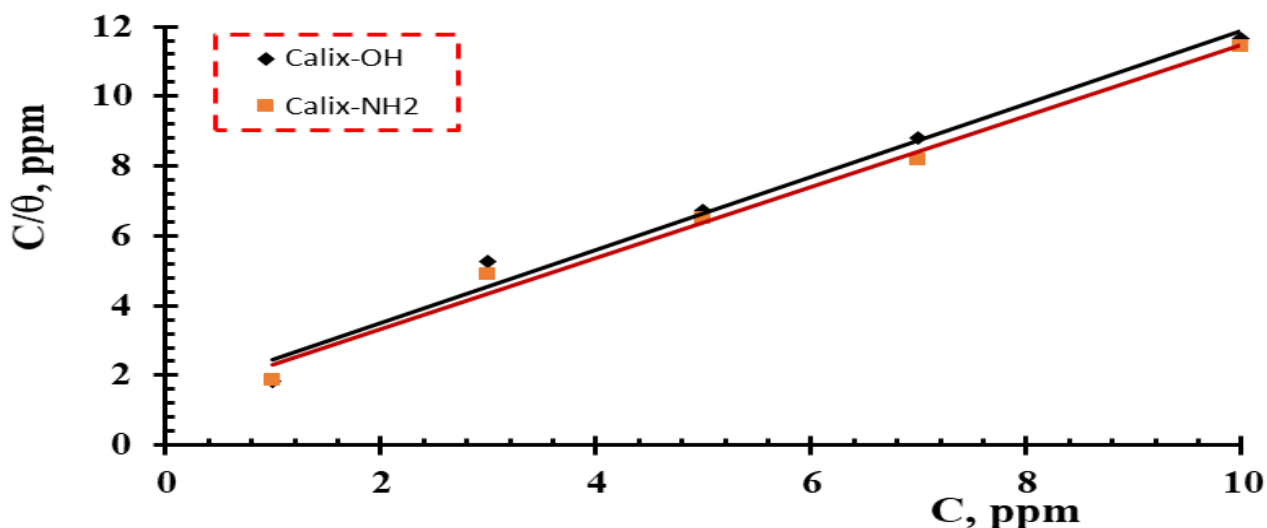

Figure 5. Langmuir adsorption isotherm based on potentiodynamic polarization measurements at 30 °C.

The calculated values of both K_{ads} and ΔG_{ads}^o [25, 32] are listed in Table (2). Data from Table (2) reveals that the adsorption of both Calix-OH and Calix-NH$_2$ compounds is physisorption as well as, the higher value of K_{ads} and more negative value of ΔG_{ads}^o in case of Calix-NH$_2$ suggests the strong and spontaneous adsorption of this compound on an aluminum surface.

Table 2. Thermodynamic parameters of the adsorption process based on the Langmuir adsorption isotherm calculated from potentiodynamic polarization measurements at 30 °C.

Inhibitor	K_{ads}, (ppm)$^{-1}$	ΔG_{ads}^o, (kJ/mol)
Calix-OH	0.85	-34.4
Calix-NH$_2$	1.16	-35.1

3.5. Computational calculations

3.5.1. Ground state geometry:

The optimized geometry of the studied Calix-OH and Calix-NH$_2$ compounds using B3LYP/6-311G (d,p) level of theory shows cone structure for both compounds as shown in Figure (6). The oxygen atoms of the OH groups in Calix-OH compound form a square structure with 2.656 A with O-O diagonals of 3.756 A. The Sulfur atoms of the -SO$_3$H also took the square structure with 7.668 A

and S-S diagonals of 10.845 A. It has been shown the Calix-OH compound is highly symmetric. On the other hand, substitution of two hydrogens in the hydroxyl groups with–CH_2-CH_2-NH_2 made some distortion in the structure of Calix-NH_2 compound.

Calix-OH   **Calix-NH₂**
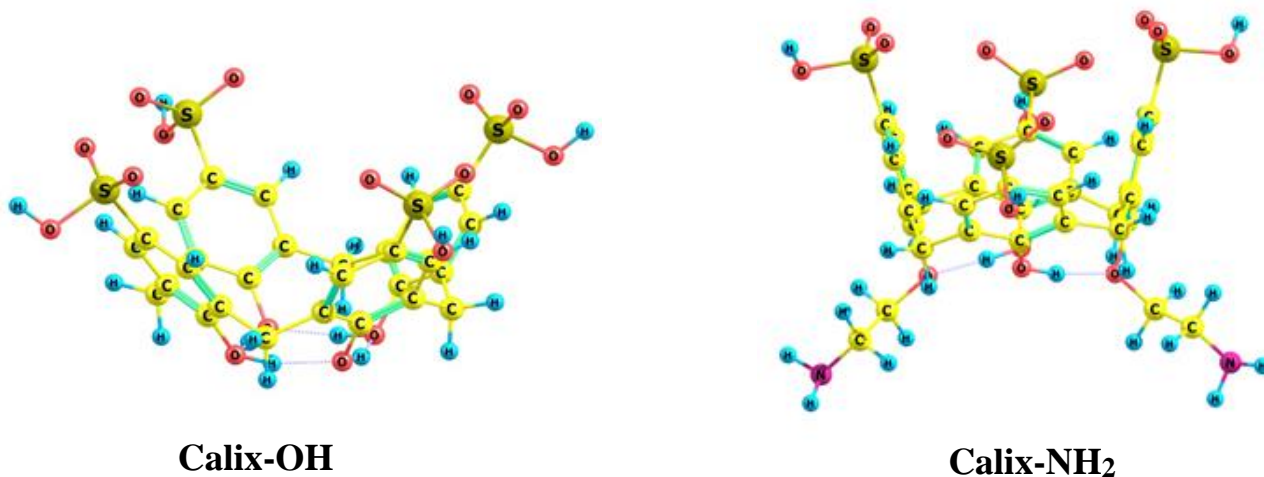
Figure 6. The optimized structure, of Calix-OH and Calix-NH₂ using B3LYP/6-311G (d,p) level of theory

The square structure of two OH groups is changed to a rectangular structure with 3.103 and 2.756 A with diagonals of 3.219 and 4.832 A, while the higher value of O-O diagonal is observed in Calix-NH_2 compound. In the same way, the square of the sulfur atoms is changed to a rectangular of 7.204 and 7.917 A with diagonals of 7.726 and 12.545 A. Also, the inserting of –CH_2-CH_2-NH_2 group narrowed the cone structure of Calix-NH_2. The R-NH_2 is shown to be directed outside so, the S-S diagonal distance that corresponded to these substitutions is decreased and this is shown from the diagonal of 7.726 Angstrom value while the other diagonal is increased.

3.5.2 Energetics:

The total energy and the zero-point energy (ZPE) of the studied compounds with various thermodynamics corrections are applied and presented in Table (3). The presence of –CH_2-CH_2-NH_2 group in Calix-NH_2 increases the zero-point energy by 0.1456 au (383 kJ/mol) compared to Calix-OH compound. Increasing the ZPE destabilized Calix-NH_2 compound i.e. increases its reactivity and this in a good agreement with the energy gab between the highest occupied molecular orbital (HOMO) and lower occupied molecular orbital (LUMO). Energies of HOMO, LUMO and energy gap ($\Delta E = E_{LUMO} - E_{HOMO}$) as well as the ionization energy (I.E) and the electron affinity (E.A) of Calix-OH and Calix-NH₂ are tabulated in Table (3). Data shows that the ionization energy of Calix-OH compound is 7.28259 eV, while the presence of –CH_2-CH_2-NH_2 group in Calix-NH_2 decreases its value to 6.77945 eV. So, we can conclude that the oxidative power is decreased upon the substitution and this is reflected on their energy gab values. The ΔE of Calix-OH compound is calculated to be 5.31575 eV which is decreased to 5.06894 eV in Calix-NH_2 compound. Moreover, the electron affinity of Calix-OH is 1.96684 eV while 1.71051 eV for Calix-NH₂.

Table 3. The total energy of the Studied compounds after various thermodynamics and zero-point energy corrections are applied, calculated using B3LYP/6-311G (d,p) level of theory

G.S. Properties	Calix-OH	Calix-NH$_2$
E_0(au)	-3878.25449	-4146.21990
E_0 (Kcal/mol)	-2433641.95486	-2601792.82426
E_0 (KJ/mol)	-10182357.93910	-10885901.17670
EZPE (au)	0.51050	0.65629
Hcorr(au)	0.55561	0.71101
Gcorr(au)	0.42846	0.56145
E_0 + EZPE(au)	-3877.74399	-4145.56362
E0 + Hcorr(au)	-3877.69888	-4145.50889
E0 + Gcorr(au)	-3877.82603	-4145.65846
Dipole Moment D	12.46650	16.19320
E_{HOMO} [a]	-0.26763	-0.24914
I,eV	7.28259	6.77945
E_{HOMO-1}	-0.27472	-0.25452
E_{LUMO} [b]	-0.07228	-0.06286
A, eV	1.96684	1.71051
E_{LUMO+1}	-0.06791	-0.06000
ΔE, eV	5.31575	5.06894

[a] I.E. = - EHOMO,   [b] E. A. = - ELUMO, $\Delta E = E_{LUMO} - E_{HOMO}$

The adsorption behaviour of these compounds can be concluded from the E.A. values. Increasing the values of the electron affinity, decreases the adsorption power on the metal surface, so, it is expected that, the Calix-NH$_2$ compound will be of the higher adsorption energy on aluminum surface that be agreed with the calculated thermodynamic adsorption parameters. The band gap energy (ΔE) signifies the reactivity of the molecules. The values of the ΔE of the two compounds are presented in Table (3) show that the reactivity increases over the substitution by R-NH$_2$ group since it has the lower energy gab value. As a result, the passivation (inhibition power) is increased over the substitution. Also, one could say that, the presence of R-NH$_2$ groups acts as a higher weight on the molecule than the –OH group. And, as a result the adsorption energy in case of R-NH$_2$ substitution is of higher value than the parent compound and this is confirmed with the lower ΔE value. The dipole moment values measure the polarizability of the molecules. As a result of the distortion of the parent by adding R-NH$_2$ group increases the dipole moment increases as found in Table (4).

3.5.3. Frontier Molecular orbitals:

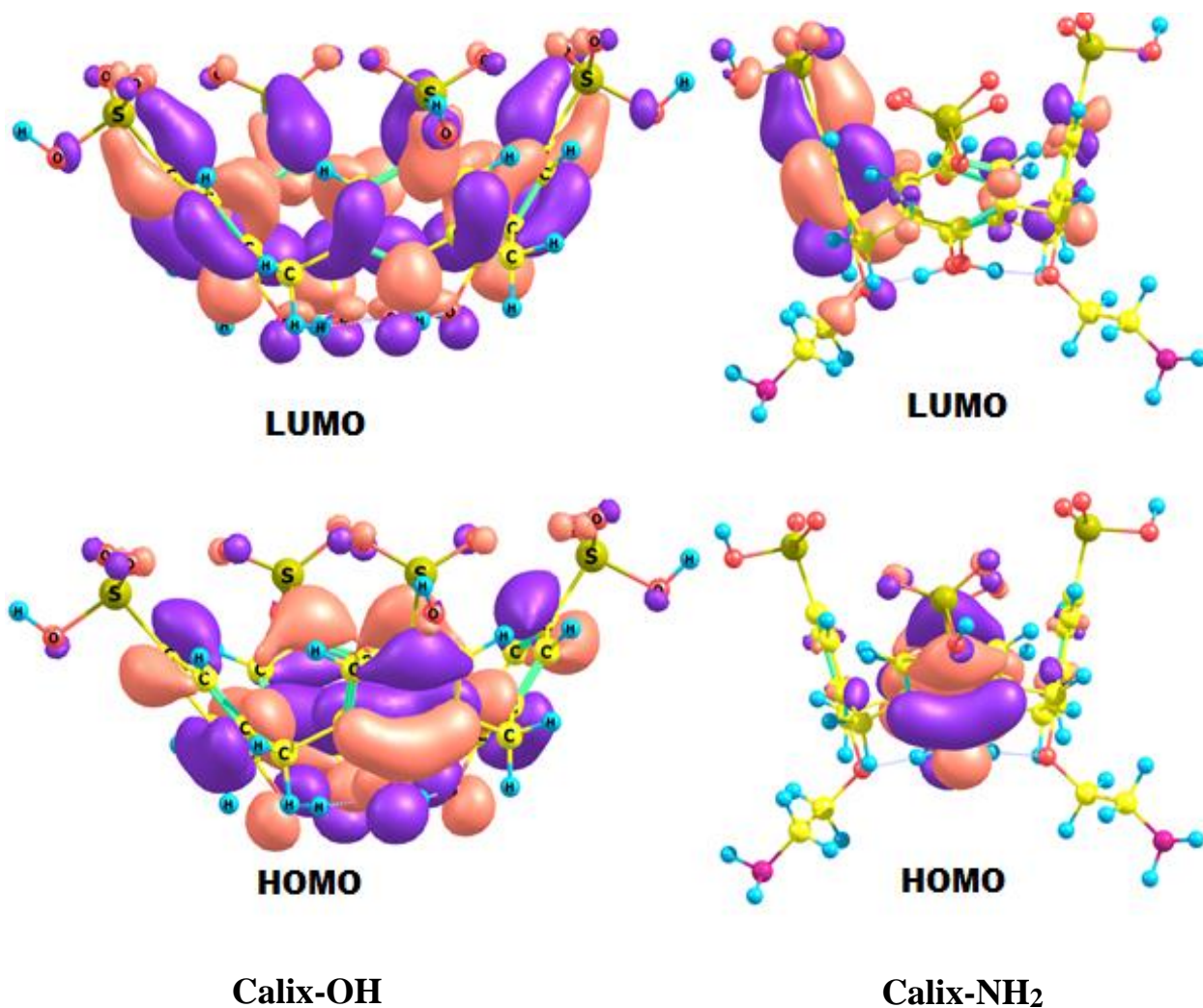**Calix-OH**   **Calix-NH₂**

Figure 7. The highest occupied molecular orbitals and the lowest unoccupied molecular orbitals (HOMO and LUMO Frontier orbitals) for both compounds using B3LYP/6-311G (d,p) level of theory

The Frontier molecular orbitals of HOMO's and LUMO's of Calix-OH and Calix-NH₂ compounds are visualized in Figure (7). It is shown that the HOMO of the parent compound is delocalized over the whole molecule but in case of the R-NH₂ substitution, it is localized on the center of the molecule and it is far from the R-NH₂ groups and the corresponding –SO₃H groups. Looking to the LUMO's, it is found that the LUMO of the parent compound is delocalized over the whole molecule while the LUMO of the R-NH₂ derivative is localized on one side of the molecule. So, going from HOMO to LUMO for these compound involves charge transfer.

3.5.4. Natural charges and Molecular Surfaces:

The natural charge density (NCD) distribution of Calix-OH and Calix-NH₂ is present in Figure (8). It is clear that the oxygen atoms show highly negative center, but the negative charge density of

the oxygen of the –SO₃H groups are more negatively charged compared to the oxygen of the –OH groups. Actually there are no big differences between the charge density between the two compounds as shown from the NCD numbers in Figure (8).

Calix-OH   **Calix-NH₂**
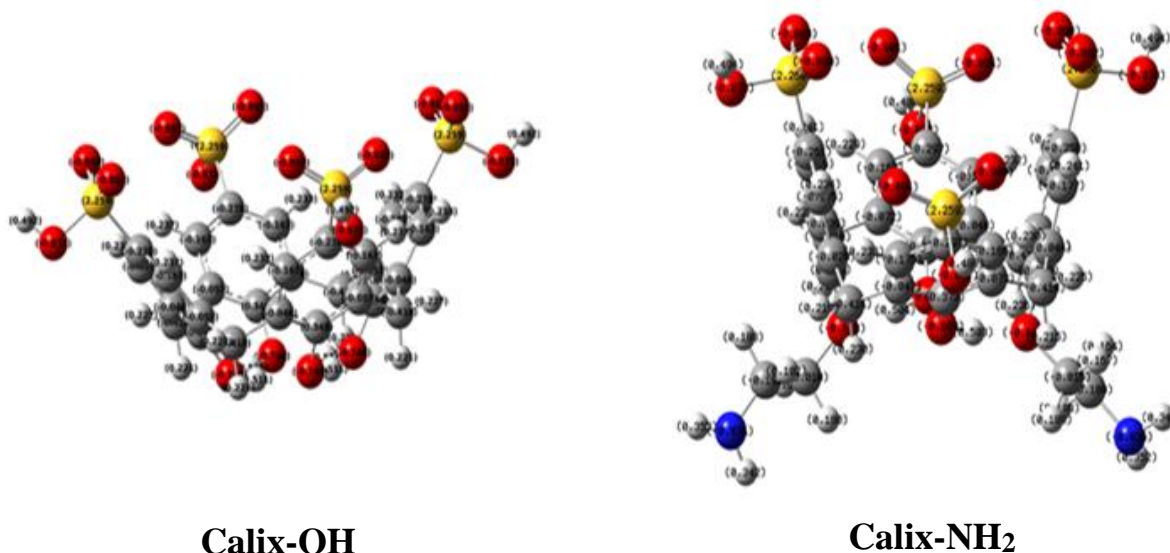
Figure 8. Natural charge distribution of compounds using NBO analysis using B3LYP/6-311G (d,p) level of theory

The electro static potential (ESP) on the iso-electron density surface can be mapped using the MEP method. The molecular size, molecular geometry and negative centers were displayed in terms of color grading. The cone structure of the studied compounds is clearly appeared from the ESP surface. The color scheme for the ESP ranges from - 0.06 (for the red color) to + 0.06 (for the blue color). Where, the high electron density area is presented in red and yellow colors while the electron density deficiency is shown in blue and light blue colors.
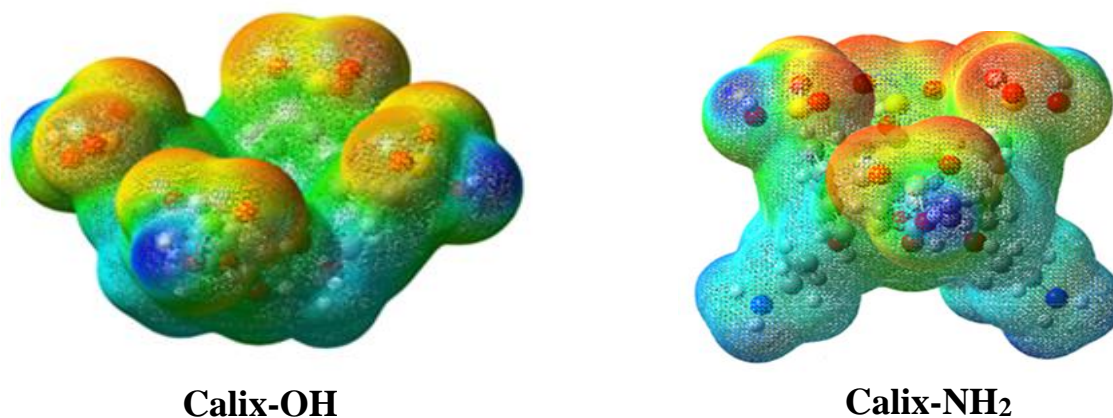

Calix-OH   **Calix-NH₂**

Figure 9. Electro static potential (ESP) of both molecules using B3LYP/6-311G (d,p) level of theory from -0.06 to +0.06.

The zero potentials (neutral centers) are shown in green color. The calculations confirmed that, the electron-rich centers are referred to the lone pairs electronegative atoms especially on the oxygen of the –SO₃H groups. The intensity of the red color in both compounds is more intense in Calix-NH₂

compared to Calix-OH as shown in Figure (9) that be agreed with the calculated NCD. It can be concluded that the presence of R-NH$_2$ in Calix-NH$_2$ increases its electron density, so increases its electrostatic attraction with aluminum surface and consequently its protection efficiency. This finding is agreed well with the experimental data. The intensity of the red color in both compounds is more intense in Calix-NH$_2$ compared to Calix-OH as shown in Figure (9) that be agreed with the calculated NCD. It can be concluded that the presence of R-NH$_2$ in Calix-NH$_2$ increases its electron density, so increases its electrostatic attraction with aluminum surface and consequently its protection efficiency. This finding is agreed well with the experimental data.

4. CONCLUSION

1- Corrosion protection of aluminum in 2M H$_2$SO$_4$ solution is investigated using water-soluble calix [4] arenes compounds at 30 °C by electrochemical techniques and DFT calculations.
2- Electrochemical measurements reveal that Calix-OH and Calix-NH$_2$ shift both the open circuit and corrosion potentials to more noble values and the maximum inhibition efficiency is found to be for Calix-NH$_2$.
3- Aluminum/electrolyte interface in case of Calix-NH$_2$ behaves as more ideal capacitive structure rather than that in case of Calix-OH.
4- The best fit adsorption isotherm is found to be Langmuir adsorption isotherm with physical nature.
5- DFT calculations clarified that the presence of R-NH$_2$ in Calix-NH$_2$ increases its natural charge density that increases its electrostatic attraction with aluminum surface.

References

1. C. D. Gutsche and J. A. Levine, *J. Am. Chem. Soc*., 104 (1982) 265.
2. S. Kanamathareddy and C. D. Gutsche, *J. Org. Chem.,* 60 (1995) 6070.
3. P. Jose and S. Menon, *Bioinorg. Chem. Appl.*, 2007 (2007) 65815.
4. R. Rodik, S. Cherenok, O. Kalchenko, O. Yesypenko, J. Lipkowski, and V. Kalchenko, *Curr. Org. Chem.*, 22 (2018) 23.
5. A. Mohammadi, M. M. Lakouraj and M. Barikani, *RSC Advances*, 6 (2016) 87539.
6. A. Mohammadi, M. Barikani, A. H. Doctorsafaei, A. P. Isfahani, E. Shams, B. Ghalei, *Chem. Eng. J.*, 349 (2018) 466.
7. B. Fan, H. Hao, B. Yang, Y. Li, *Res Chem Intermed*, 44 (2018) 5711.
8. M. Kaddouri, N. Cheriaa, R. Souane, M. Bouklah, A. Aouniti, R. Abidi, B. Hammouti, J. Vicens, *J. Appl. Electrochem.*, 38 (2008) 1253.
9. M. Kaddouri, S. Rekkab, M. Bouklah, B. Hammouti, A. Aouniti, Z. Kabouche, *Res. Chem. Intermed.*, 39 (2013) 3649.
10. M. M. El-Deeb, E. N. Ads and J. R. Humaidi, *Int. J. Electrochem. Sci.*, 13 (2018) 4123.
11. M. M. EL-Deeb, H. M. Alshammari and S. Abdel-Azeim, *Can. J. Chem.*, 95 (2017) 612.

12. C. D. Gutsche, B. Dhawan, K. H. No and R. Muthukrishnan, *J. Am. Chem. Soc.*, 103 (1981) 3782.
13. C. Wieser, C. B. Dieleman and D. Matt, *Coord. Chem. Rev.*, 165 (1997) 93.
14. E. S. Español and M. M. Villamil, *Biomolecules*, 9 (2019) 90.
15. C. D. Gutsche and L. –G. Lin, *Tetrahedron*, 42 (1986) 1633.
16. S. Shinkai, K. Araki, T. Tsubaki, T. Arimura and O. Manabe, *J. Chem. Soc. Perkin Trans. 1*, 1987 (1987) 2297.
17. H. Halouani, I. Dumazet-Bonnamour, M. Perrin and R. Lamartine, *J. Org. Chem.*, 69 (2004) 6521.
18. R. Chebrolu Pulla and A. Amitabha, *Indian Pat. Appl.*, (2013) IN 2011MU01089 A 20130111.
19. Gaussian 03, Revision C.02, M. J. Frisch, G. W. Trucks, H. B. Schlegel, G. E. Scuseria, M. A. Robb, J. R. Cheeseman, J. A. Montgomery, Jr., T. Vreven, K. N. Kudin, J. C. Burant, J. M. Millam, S. S. Iyengar, J. Tomasi, V. Barone, B. Mennucci, M. Cossi, G. Scalmani, N. Rega, G. A. Petersson, H. Nakatsuji, M. Hada, M. Ehara, K. Toyota, R. Fukuda, J. Hasegawa, M. Ishida, T. Nakajima, Y. Honda, O. Kitao, H. Nakai, M. Klene, X. Li, J. E. Knox, H. P. Hratchian, J. B. Cross, V. Bakken, C. Adamo, J. Jaramillo, R. Gomperts, R. E. Stratmann, O. Yazyev, A. J. Austin, R. Cammi, C. Pomelli, J. W. Ochterski, P. Y. Ayala, K. Morokuma, G. A. Voth, P. Salvador, J. J. Dannenberg, V. G. Zakrzewski, S. Dapprich, A. D. Daniels, M. C. Strain, O. Farkas, D. K. Malick, A. D. Rabuck, K. Raghavachari, J. B. Foresman, J. V. Ortiz, Q. Cui, A. G. Baboul, S. Clifford, J. Cioslowski, B. B. Stefanov, G. Liu, A. Liashenko, P. Piskorz, I. Komaromi, R. L. Martin, D. J. Fox, T. Keith, M. A. Al-Laham, C. Y. Peng, A. Nanayakkara, M. Challacombe, P. M. W. Gill, B. Johnson, W. Chen, M. W. Wong, C. Gonzalez, and J. A. Pople, *Gaussian, Inc., Wallingford CT*, (2004).
20. A. D. Becke, *J. Chem. Phys.*, 104 (1996) 1040.
21. A. D. Becke, *J. Chem. Phys.*, 107 (1997) 8554.
22. K. Raghavachari, G. W. Trucks, J. A. Pople, M. Head-Gordon, *Chem Phys Lett*, 157 (1989) 479.
23. A. D. Becke, *J. Chem. Phys.*, 98 (1993) 5648.
24. M. M. El-Deeb, S. M. Sayyah, S. S. Abd El-Rehim and S. M. Mohamed, *Arabian J. Chem.*, 8 (2015) 527.
25. M. M. El-Deeb, N. S Abdel-Shafi and A. H. Shamroukh, *Int. J. Electrochem. Sci.*, 13 (2018) 4123.
26. P. Arellanes-Lozada, O. Olivares-Xometl, D. Guzmán-Lucero, N. Likhanova, M. Domínguez-Aguilar, I. Lijanova, E. Arce-Estrada, *Materials*, 7 (2014) 5711.
27. A. Y. El-Etre, *Corros. Sci.*, 45 (2003) 2485.
28. M. M. El-Deeb, E. N. Ads and J. R. Humaidi, *Int. J. Electrochem. Sci.*, 13 (2018) 4123.
29. H. Rahmani, K. I. Alaoui, K.M. Emran, A. El Hallaoui, M. Taleb, S. El Hajji, B. Labriti, E. Ech-chihbi, B. Hammouti and F. El-Hajjaji, *Int. J. Electrochem. Sci.*, 14 (2019) 985.
30. G. Bereket, E. Hur and C. O. Retir, J. Mol. Struct., 578 (2002) 79.
31. B. A. Boukamp, *Solid State Ionics*, 20 (1986) 31.
32. S. M. Sayyah, M. M. El-Deeb, S. S. Abd El-Rehim, R. A. Ghanem and S. M. Mohamed, *Port. Electrochim. Acta*, 32 (2014) 417.